European Journal of Radiology 119 (2019) 108634

Contents lists available at ScienceDirect

European Journal of Radiology

journal homepage: www.elsevier.com/locate/ejrad

Research article

Computational quantitative MR image features - a potential useful tool in differentiating glioblastoma from solitary brain metastasis

Katarina Petrujkić[a,*], Nebojša Milošević[c], Nemanja Rajković[c], Dejana Stanisavljević[d], Svetlana Gavrilović[a], Dragana Dželebdžić[a], Rosanda Ilić[e,f], Antonio Di Ieva[g], Ružica Maksimović[a,b]

[a] Clinical Centre of Serbia, Centre for Radiology and Magnetic Resonance, Pasterova 2, Belgrade 11000, Serbia
[b] Department of Radiology, School of Medicine, University of Belgrade, Dr Subotića 8, Belgrade 11000, Serbia
[c] Department of Biophysics, School of Medicine, University of Belgrade, Višegradska 26/2, Belgrade 11000, Serbia
[d] Department for Medical Statistics, School of Medicine, University of Belgrade, Dr Subotića 8, Belgrade 11000, Serbia
[e] Department of Neurosurgery, School of Medicine, University of Belgrade, Dr Subotića 8, Belgrade 11000, Serbia
[f] Clinical Centre of Serbia, Clinical for Neurosurgery, Dr Koste Todorovića 54, 11000 Belgrade, Serbia
[g] Department of Clinical Medicine, Faculty of Medicine and Health Science, Neurosurgery Unit, Macquarie University, 2 Technology Place, Macquarie University, Sydney, NSW 2109, Australia

ARTICLE INFO

Keywords:
Glioblastoma
Metastasis
MRI
Texture analysis
Fractal analysis

ABSTRACT

Purpose: Glioblastomas (GBM) and metastases are the most frequent malignant brain tumors in the adult population. Their presentation on conventional MRI is quite similar, but treatment strategy and prognosis are substantially different. Even with advanced MR techniques, in some cases diagnostic uncertainty remains. The main objective of this study was to determine whether fractal, texture, or both MR image analyses could aid in differentiating glioblastoma from solitary brain metastasis.

Method: In a retrospective study of 55 patients (30 glioblastomas and 25 solitary metastases) who underwent T2W/SWI/CET1 MRI, quantitative parameters of fractal and texture analysis were estimated, using box-counting and gray level co-occurrence matrix (GLCM) methods.

Results: All five GLCM parameters obtained from T2W images showed significant difference between glioblastomas and solitary metastases, as well as on CET1 images except correlation (S_{COR}), contrary to SWI images which showed different values of two parameters (angular second moment-S_{ASM} and contrast-S_{CON}). Only three fractal features (binary box dimension-D_{bin}, normalized box dimension-D_{norm} and lacunarity-λ) measured on T2W and D_{norm} measured on CET1 images significantly differed GBMs from solitary metastases. The highest sensitivity and specificity were obtained from inverse difference moment (S_{IDM}) on T2W and S_{IDM} on CET1 images, respectively. Combination of several GLCM parameters yielded better results. The processing of T2W images provided the most significantly different parameters between the groups, followed by CET1 and SWI images.

Conclusions: Computational-aided quantitative image analysis may potentially improve diagnostic accuracy. According to our results texture features are more significant than fractal-based features in differentiation glioblastoma from solitary metastasis.

1. Introduction

Differentiating a glioblastoma (GBM) from a cerebral metastasis is a common radiological challenge, especially in patients without proven systemic malignancy and with solitary lesion. These two entities, as the most frequent malignant brain tumors in the adult population, share some overlapping features on diagnostic imaging, but require substantially different treatment strategy. On conventional magnetic resonance (MR) imaging, both glioblastomas and brain metastases feature a mass with ring-like contrast-enhancement, central necrosis and

Abbreviations: GBM, glioblastoma multiforme; GLCM, gray level co-occurrence matrix; FD, fractal dimension; EGFR, epidermal growth factor receptor; ROI, region of interest; MIPAV, medical image processing, analysis and visualization

* Corresponding author at: Clinical Centre of Serbia, Centre for Radiology and Magnetic Resonance, Pasterova 2, Belgrade 11000, Serbia.
E-mail address: r_katarina@yahoo.com (K. Petrujkić).

https://doi.org/10.1016/j.ejrad.2019.08.003
Received 14 January 2019; Received in revised form 28 July 2019; Accepted 5 August 2019

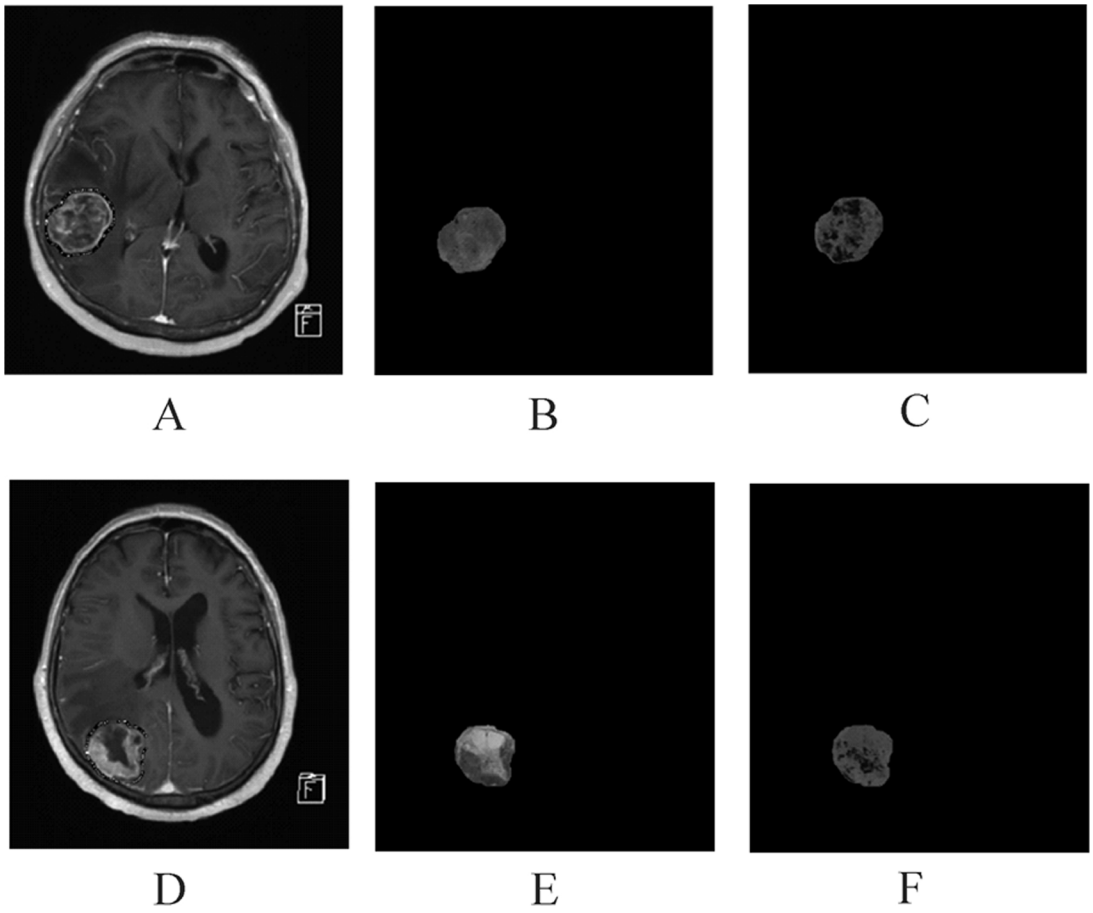

Fig. 1. Contoured tumor, glioblastoma (A-C) and metastasis (D-F), on T1 postcontrast MR image (A, D), segmented tumor on T2W (B, E) and SWI image (C, F).

surrounding edema. Advanced MR techniques, such as magnetic resonance spectroscopy (MRS), diffusion and perfusion MRI, and PET scans as well, are useful to improve differential diagnosis, helping in evaluating the physiologic and metabolic profile of both the tumor and peritumoral area. Even with these techniques performed, in some cases diagnostic uncertainty remains [1,2,3].

Considering the overlapping MR imaging features of GBM and solitary brain metastasis, in our study we aimed to quantify the MRI features of GBM and metastases. In order to achieve such a task, we have included fractal and texture analysis, along to standard morphometric computational analysis.

Fractal geometry has been applied to neuroimaging for lesion detection, features extractions, pattern recognition and morphologic quantitative studies. It provides a mathematical assessment of morphological characteristics (e.g. roughness and geometric complexity) of the brain in its entire physiopathological spectrum, including brain tumors [4,5]. Fractal parameters of medical image analysis were used for tumor classifications [6,7,8,9], treatment follow-up [10] and even more as reliable prognostic factors of patient survival [11].

Texture analysis is based on numerous mathematical methods that allow pattern evaluation of the gray-level and pixel positions in medical images. It has been shown as an effective way of assessing tumor heterogeneity, as described in studies related to breast [12], lung [13] and colorectal cancers [14], as well as to brain tumors, including GBM and metastases [15,16,17].

In this study our primary aim was to determine whether fractal, texture, or both MR image analyses could aid in differentiating GBM from solitary metastasis. In addition, standard morphometric (Euclidean) parameters were evaluated as well.

2. Materials and methods

2.1. Patient group

Our study included two groups of patients who underwent MRI during the 4-year period (2014 -2017) at the institution, approved by it's Ethics Committee (Approval No: 630/4). The first group included 30 patients (15 men, age range 40-70, and 15 women, age range 50-75), with histologically proven GBM. The second group included 25 patients (17 men, age range 51-83, and 8 women, age range 51-75) with brain metastases of different origin (11 pulmonary carcinomas, 7 mammary, 4 colon, 2 melanomas, 1 renal). In this patient group, the definitive diagnosis of brain metastasis was confirmed by other diagnostic and laboratory tests, or histologically, in patients who underwent surgical resection.

Exclusion criteria were: multiple lesions (multicentric/multifocal glioblastoma, multiple metastases), secondary GBM (i.e., GBM developed from a known pre-existing lower grade tumor), GBM with contralateral spread, hemorrhagic lesions (e.g., homogenously "black" on SWI) and post-radiation treatment metastases. In particular, this study included only patients with solitary contrast-enhancing lesion with central necrosis and intratumoral SWI signal, which is a classical differential diagnostic dilemma from the initial MRI, later confirmed as GBM or metastasis.

2.2. Image acquisition and preparing for analysis

All MRIs were performed on the 3 T MR unit (Magnetom Skyra, Siemens, Germany). Conventional imaging sequences, used for further analysis were: contrast-enhanced (CE) 3D T1 MPRAGE images (matrix

of 256 × 256, voxel-size of 0.9 × 0.9 × 0.9 mm; 192 slices, TR/TE of 2300/2.32 ms, TI of 900 ms; Magnevist-gadopentetate dimeglumine 0.5 mmol/ml, Bayer, application dose 2 ml/10 kg of body weight), T2-weighted Turbo Spin Eho images (matrix of 270 × 320, voxel-size of 0.7 × 0.7 × 5 mm, 25 slices, TR/TE of 6000/99 ms, echo train length of 9), and 3D SWI images (image matrix of 252 × 288, voxel-size of 0.8 × 0.8 × 1.5 mm, TR/TE of 28/20 ms, 96 slices).

Axial images (one same section on three different sequences), representing a tumor with all its characteristic imaging features (solid contrast-enhancing component, necrosis, pathological vascularisation), were selected and extracted in TIFF format using a MicroDicom viewer (available on www.microdicom.com). Each tumor was outlined, by consensus of two neuroradiologists, on the CET1 image, considering its superior tumor margin compared to T2W and SWI images. All images had the same dimensions (width and height) and the same resolution. Subsequently, the resulting Region of Interest (ROI) was over imposed to corresponding T2W and SWI images. Finally, the tumor representation in these three sequences was segmented (Fig. 1). The MIPAV (Medical Image Processing, Analysis and Visualization, available on http://mipav.cit.nih.gov/) software was used for all of the above steps.

As stated previously (Subsection 2.1), the study group consisted of 55 patients, recorded in three sequences encompassing a total of 165 images. Each image, was uploaded in the public domain software for image analysis *Image J* (https://imagej.nih.gov/ij/) for further quantitative analysis. Specifically, program recognized cropped image of the tumor (from Fig. 1) as a RGB image (Fig. 2A), with combination of gray and black (in and outside tumor area) pixels. Then, this image was converted in 8 bit grayscale (Fig. 2B), where all black pixels were digitally removed.

The next step in preparing images included obtaining binary image of the selection and the border of whole area of the tumor. Each grayscale image (Fig. 2B) was transformed in binary (Fig. 2C) with specialized command ('Make Binary'), with the level threshold which was dependent on the signal intensity on grayscale image. Further, a grayscale image (Fig. 2B) was selected (with 'Wand tool'), converted into binary, and all regions of the tumor was filled with black pixels (Fig. 2D). Finally, a specific command ('Binary: Outline') was used to create an outline image of the tumor (Fig. 2E). This procedure was done in the same way in all three sequences. All stages of image processing were done by two physicist (specialist in image analysis). All further measurements (computational and texture) were done by *Image J*, using particular command, standard tools or specific plugins. As a result, the tumor morphology was quantified with fourteen morphometric parameters divided in two categories: computational (9) and texture (5) parameters.

2.3. Analysis of the binary image

The morphology of the binary image of the entire tumor, and its interior, were quantified using 4 Euclidean and 5 fractal parameters. Euclidean parameters were the surface area (A), shape or perimeter (P), space-filling ratio (SF_R) and asymmetry index or circularity of the tumor projection (M). Using binary image of the whole projection (Fig. 2D), the A and P was calculated and expressed in pixels. The SF_R was obtained dividing number of pixels on Fig. 2D with number of pixels when whole frame on Fig. 2D was filled with black pixels. Finally, the M was obtained with formula $4A/P^2$ [18].

Fractal parameters were obtained using box-counting method. Among various fractal methods [19], the box-counting [20,21] appears to be the method which suitably measures fractal dimensions of natural objects [22,23]. Theoretically, for a subset F ($F \subset R^n$), the box dimension of F approximately linearly depends on $N\delta(F)$, i.e. the smallest number of closed balls of radius δ that cover F or the largest number of disjoint balls of radius δ with centers in F [24], with assumption that lower and upper box dimensions are equal. This method, applied on digitized images in the plane, covers the image with a grid of square cells with cell size r [21]. Firstly, digitized image must be converted to binary and the cell size must be expressed as the number of pixels [25].

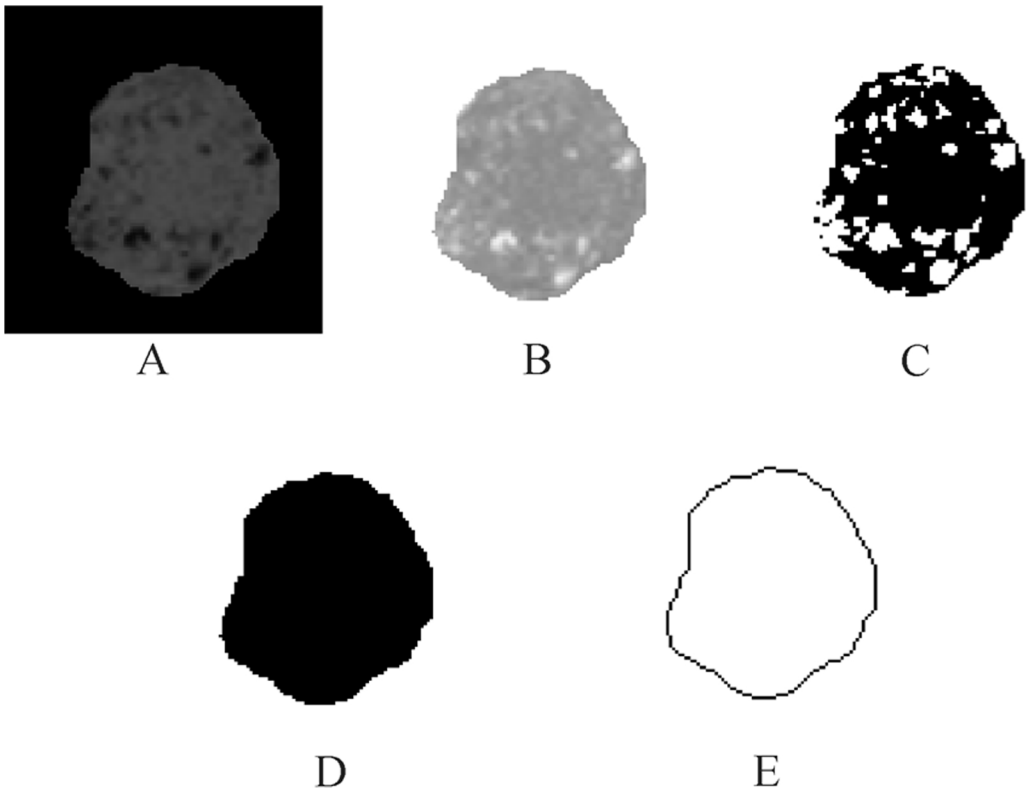

Fig. 2. Postprocessing of cropped SWI image: TIFF image with black background (A), grayscale image (B), grayscale image converted in binary (C), binary image of whole tumor (D) and outline image (boundary) of whole tumor (E).

What is more, the box sizes should be taken as geometric progression, from 2^0 to 2^k pixel, where k is the value for which N is equal to one [23].

Five fractal parameters, that indirectly quantify the surface area, shape, both translational and rotational invariance of the image [22], were obtained in *Image J*, either with command of the software or with FracLac plugin [26]. The binary box dimension (D_{bin}) was obtained with command ('Standard Box Count') on Fig. 2C, while outline box dimension (D_{out}) was obtained on Fig. 2E. The normalized box dimension (D_{norm}) was obtained when two box dimensions on Fig. 2D were calculated and divided. First dimension was calculated on the image of whole tumor and second dimension was calculated when whole image was filled with black pixels. Last two parameters (differential box dimension-D_{diff} and lacunarity-λ) were obtained with FracLac plugin on grayscale images Fig. 2B. Here, FracLac calculated these parameters from the relationships between the change in average intensity of pixels and the change in grid caliber [26].

2.4. Analysis of the grayscale image

A digital image in grayscale mode can be most effectively quantified using some of the textural analysis techniques. In general, texture image analysis contains information that quantifies the distribution of gray color within a group of pixels. Precisely, image texture can express: i) the homogeneity of the tones in the image, ii) the linear connection of the tones, iii) the contrast of the image, iv) the boundary between the gray tones and v) the complexity of the distribution of the tones [27].

One of the well-known texture techniques is GLCM. It is a two-dimensional gray tone histogram for a selected pair of pixels, separated by a fixed spatial distance in the form of a matrix [28]. This technique calculates, among others, five significant parameters i.e. second order statistical moments [25]: the angular second moment (S_{ASM}), the inverse difference moment (S_{IDM}), the contrast (S_{CON}), the correlation (S_{COR}) and the entropy (S_{ENT}). Their mathematical definitions and detailed explanations can be found in Djuričić et al [29].

The five GLCM parameters were obtained with *Texture Analyzer* plugin of *Image J* on grayscale image, i.e. on Fig. 2B [30]. The plugin was attuned as follows: the pixel distance was set to 1 and isotropic spatial orientation obtained by averaging the feature values at 0 and 90° angles, in order to normalize images. For each image, the plugin calculated five parameters [27] which describe texture uniformity of the image (S_{ASM}), local homogeneity of the image (S_{IDM}), spatial frequency of the gray tones in the image (S_{CON}), distribution of gray tones in the image (S_{COR}) and amount of information combined with complexity of the image (S_{ENT}). Fig. 3 shows the values of five GLCM parameters for one patient with GBM (Fig. 3, left) and the other with solitary metastasis (Fig. 3 right) in three different sequences. The provided example (Fig. 3) shows that the most notable differences between the two tumor types were spatial frequencies of the gray tones and local homogeneity of the images. The formulas and the description of GLCM texture parameters are included in *Supplement 1* of this article [31].

2.5. Statistical analyses

Distribution of data was tested using Shapiro-Wilk test (results are presented in *Supplement 2* along with the results of testing of parameters with normal distribution, *Supplement 3*). The difference between two groups of parameters (group with glioblastomas and group with solitary metastases) was statistically analyzed by Mann-Whitney (U) test. A value of $p < 0.05$ was considered statistically significant. Classification was evaluated with the area under receiver operating characteristic curve (AUROC) considering two strategies: multiclass and one-versus-one. The SPSS software package v23 (IBM SPSS Statistics, Chicago, IL, USA, demo version) was employed for statistical analysis.

3. Results

The results are presented in Tables 1–3 according to the analyzed sequences (SWI, CET_1 and T_2W respectively). The medians and ranges of 14 parameters for the two groups of the brain tumors (GBMs and metastases) in SWI sequence and their statistical analysis is shown in Table 1. In this sequence, all Euclidean parameters (A, P, SF_R and M) were significantly different between groups, while only two GLCM parameters (S_{ASM} and S_{CON}) were different and none of the fractal features has found to be significantly different. In CET_1 sequence (Table 2), besides the significant difference in all Euclidean parameters, one fractal parameter (D_{norm}) as well as four of GLCM parameters (S_{ASM}, S_{IDM}, S_{CON}, S_{ENT}) were significantly different. Finally, the analysis of T_2W sequence yielded the best results (Table 3), with significantly different values of all Euclidean, all GLCM parameters (S_{ASM}, S_{IDM}, S_{CON}, S_{COR}, S_{ENT}) and the three fractal parameters (D_{bin}, D_{norm} and Λ).

Observing all three sequences, a significant difference between groups was found in all Euclidean parameters. This result was due to the fact that its value is strictly dependent on the dimension of the ROI. The two GLCM parameters (S_{ASM} and S_{CON}) were found to be significantly different in all sequences. These results indicate that images, recorded in all three sequences, differed between the groups in texture uniformity of the image and spatial frequency of the gray tones in the images.

AUROC analyzes showed that the performance of the Euclidean, fractal and GLCM parameters in differentiating glioblastoma from solitary brain metastasis ranged from 0.657 for M to 0.795 for S_{IDM} on CET1 image. The highest sensitivity (83.3%) and the highest specificity (84%) were obtained from S_{IDM} on T2W image and S_{IDM} on CET1 image, respectively (Table 4). Cut-off was determined for the combination of highest summation of sensitivity and specificity values.

AUROC analyzes was applied on combinations of the most significant parameters/images (parameters which was on individually analysis best differentiate two kind of tumors). Combination of several GLCM parameters yielded better results, i.e. AUROC value for five GLCM parameters on three MR images (S_{IDM}/CET1,T2W, S_{ENT}/CET1, S_{ASM}/SWI,CET1,T2W, S_{CON}/T2W and S_{COR}/T2W) was 0.908 with sensitivity 86.7% and specificity 80.0% (Fig. 4A). Similar results were obtained by the combination of four GLCM parameters (S_{IDM}, S_{ASM}, S_{CON}, S_{COR}) derived from T2W MR images: AUROC 0.895, sensitivity 93.3% and specificity 76.0% (Fig. 4B). Even more the combination of three GLCM parameters (S_{IDM}, S_{ENT}, S_{ASM}) derived from CET1 MR images, gave AUROC 0.815 with sensitivity 63.3% and specificity 88.0% (Fig. 4C). On the other hand, combination of fractal parameters (i.e. D_{norm}/CET1,T2W, D_{bin}/T2W) or Euclidean parameters (A, P, SF_R) in this study provided less promising results: AUROC values 0.791 and 0.728, sensitivity 86.7% and 70.0%, specificity 72.0% and 72.0%, respectively.

4. Discussion

The four morphometric (Euclidean) MR images parameters used in our study showed promising results showing higher values of A, SF_R and P for GBMs than metastases, while median of M for GBM was lower. This result was computational demonstration of the well-known features of the "more circular shape" of metastasis and corrobates with the previos results [32,33]. For instance, Mouthuy et al [32] analyzed circularity and surface measurements and reported that metastases are often smaller, somewhat spherical with regular contours and extend outwards evenly, contrary to glioblastomas. Furthermore, Blanchet et al [33] suggested that the invasive growth of glial high-grade tumors influences the shape of the tumor enough to differentiate them.

Di Ieva et al [6] have applied fractal analysis on various tumor types/grades in search for tumor's specific morphometric parameters for quantifying differences between them. FD and signal ratio were able to discriminate low-grade from grade III and IV gliomas, metastases and

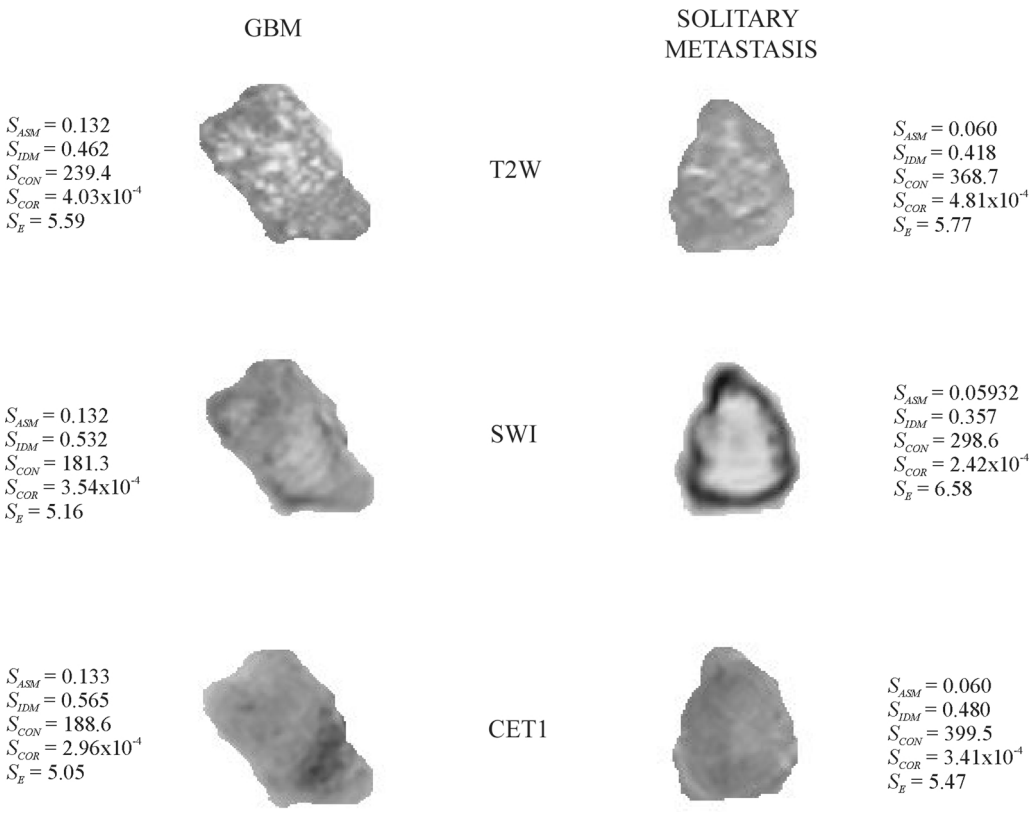

Fig. 3. Example of selected GLCM parameters values in differentiating glioblastoma from solitary brain metastasis.

Table 1
Parameters derived from SWI images in patients with GBMs and solitary brain metastases.

Parameters	GBMs	Solitary metastases	*p*
Euclidian			
Surface area (A)	7919 (12595)	3891 (15648)	< **0.001**
Perimeter (P)	297.5 (305)	206 (322)	**0.002**
Space-filling ratio (SF_R)	0.011 (0.018)	0.005 (0.022)	< **0.001**
Circularity ratio (M)	0.813 (0.313)	0.850 (0.219)	**0.023**
Binary box dimension (D_{bin})	1.713 (0.322)	1.645 (0.434)	0.130
Fractal			
Outline box dimension (D_{out})	1.124 (0.124)	1.123 (0.152)	0.973
Normalized box dimension (D_{norm})	0.950 (0.122)	0.950 (0.186)	0.249
Differential box dimension (D_{diff})	1.428 (0.202)	1.452 (0.260)	0.102
Lacunarity (λ)	0.202 (0.240)	0.210 (0.441)	0.199
GLCM			
Angular second moment (S_{ASM})	0.077 (0.180)	0.048 (0.072)	< **0.001**
Inverse difference moment (S_{IDM})	0.439 (0.289)	0.435 (0.245)	0.515
Contrast (S_{CON})	213 (311)	246 (408)	**0.039**
Correlation (S_{COR})	4.865 (6.828)	5.497 (6.774)	0.088
Entropy (S_{ENT})	5.810 (2.73)	5.660 (1.92)	0.642

Values are presented as median (range) with p value of Mann-Whitney U test.
The range is calculated as the difference between maximum and minimum values in the sample.
A value of $p <$ 0.05 was considered statistically significant, the parameters which satisfy this requirement were **bolded**.

meningiomas, whereas FD was statistically different between lymphomas and high-grade gliomas. Smitha et al [9] analyzed fluid attenuation inversion recovery (FLAIR) MR images in differentiation of gliomas. They found that the lacunarity could differentiate grade II vs. grade IV, grade I vs. grade III, grade I vs. grade IV gliomas, while FD differentiated only grade I vs. grade IV gliomas. Also, Di Ieva et al [7] have successfully applied fractal analysis on SWI images to differentiate gliomas by histological grade.

Our study demonstrated limited capability of fractal analysis in differentiating GBMs vs. metastases. Only D_{bin}, D_{norm} and λ measured on T2W images and D_{norm} measured on CET1 images showed significant difference between the two groups of tumors. More precisely, higher median values of D_{bin} and D_{norm} has been derived from T2W images for GBMs group, while for metastases group higher median values of D_{norm} and λ has been derived from CET1 and T2W images respectively. Most likely, the reason was relatively small group of patients or method of image acquisition (Subsection 2.2.), as fractal analyzes are highly dependent on the number of the analyzed images. This shortcoming will possibly clear away in the future when higher amount of data will be analyzed.

Our study has shown the significant difference between the texture features of GBMs compared to metastases suggesting that it is suitable

Table 2
Parameters derived from CET1 images in patients with GBMs and solitary brain metastases.

Parameters	GBMs	Solitary metastases	*p*
Euclidian			
Surface area (A)	7919 (12595)	3891 (15648)	< **0.001**
Perimeter (P)	297.5 (305)	206 (322)	**0.002**
Space-filling ratio (SF_R)	0.011 (0.018)	0.005 (0.022)	< **0.001**
Circularity ratio (M)	0.813 (0.313)	0.850 (0.219)	**0.023**
Binary box dimension (D_{bin})	1.619 (0.257)	1.627 (0.298)	0.194
Fractal			
Outline box dimension (D_{out})	1.124 (0.124)	1.123 (0.152)	0.973
Normalized box dimension (D_{norm})	0.888 (0.174)	0.913 (0.177)	**0.017**
Differential box dimension (D_{diff})	1.346 (0.160)	1.368 (0.279)	0.488
Lacunarity (λ)	0.248 (0.233)	0.237 (0.333)	0.122
GLCM			
Angular second moment (S_{ASM})	0.077 (0.179)	0.049 (0.074)	**0.001**
Inverse difference moment (S_{IDM})	0.468 (0.285)	0.385 (0.232)	< **0.001**
Contrast (S_{CON})	199 (718)	301 (706)	**0.019**
Correlation (S_{COR})	3.167 (8.827)	2.974 (4.291)	0.168
Entropy (S_{ENT})	5.910 (2.29)	6.280 (1.56)	**0.013**

Values are presented as median (range) with p value of Mann-Whitney U test.
The range is calculated as the difference between maximum and minimum values in the sample.
A value of $p < 0.05$ was considered statistically significant, the parameters which satisfy this requirement were **bolded**.

Table 3
Parameters derived from T2W images in patients with GBMs and solitary brain metastases.

Parameters	GBMs	Solitary metastases	*p*
Euclidian			
Surface area (A)	7919 (12595)	3891 (15648)	< **0.001**
Perimeter (P)	297.5 (305)	206 (322)	**0.002**
Space-filling ratio (SF_R)	0.011 (0.018)	0.005 (0.022)	< **0.001**
Circularity ratio (M)	0.813 (0.313)	0.850 (0.219)	**0.023**
Binary box dimension (D_{bin})	1.616 (0.455)	1.532 (0.480)	**0.004**
Fractal			
Outline box dimension (D_{out})	1.124 (0.124)	1.123 (0.152)	0.973
Normalized box dimension (D_{norm})	0.911 (0.198)	0.858 (0.227)	**0.002**
Differential box dimension (D_{diff})	1.332 (0.173)	1.360 (0.247)	0.080
Lacunarity (λ)	0.268 (0.478)	0.352 (0.509)	**0.003**
GLCM			
Angular second moment (S_{ASM})	0.077 (0.180)	0.049 (0.074)	< **0.001**
Inverse difference moment (S_{IDM})	0.483 (0.276)	0.417 (0.183)	**0.001**
Contrast (S_{CON})	298 (822)	387 (1295)	**0.006**
Correlation (S_{COR})	2.258 (5.613)	3.621 (8.478)	**0.002**
Entropy (S_{ENT})	5.780 (2.44)	6.050 (1.47)	**0.021**

Values are presented as median (range) with p value of Mann-Whitney U test.
The range is calculated as the difference between maximum and minimum values in the sample.
A value of $p < 0.05$ was considered statistically significant, the parameters which satisfy this requirement were **bolded**.

for their differentiation. S_{ENT}, S_{COR} and S_{CON} had higher average values for metastases compared to GBMs group, while the S_{ASM} and the S_{IDM} showed the opposite. Similar results were published by Mouthuy et al [32] in the study that included the same tumor groups (GBMs and solitary metastases), but the texture was analyzed on the perfusion imaging.

Other investigators explored the tumor heterogeneity by means of both 2D and 3D texture analysis in search for structural differences between brain metastases originating from different systemic cancers [17,34] or regarding primary tumor's histological type [35]. Some works have confirmed a relationship between GBM texture features and survival time [15,16,36]. The diagnostic performance of MRI texture features has been shown to be successful in grading cerebral gliomas [37] and in the differentiation of radionecrosis from tumor recurrence [38,39]. Recently, Kunimatsu et al [40] and Suh et al [41] differentiated glioblastoma from primary CNS lymphoma. Furthermore, tumour's texture features may serve as a potential imaging biomarker for pretreatment prediction of methylation status in GBM [42] and prediction of EGFR (epidermal growth factor receptor) in lower grade gliomas [43].

Based on the expected increased heterogeneity in GBM compared to the metastasis, ascribed to angiogenesis heterogeneity, texture features from CET1 images theoretically, should be significant in differentiating those tumors. However, we found that the texture features extracted from T2W images are more informative in distinguishing GBM from metastasis. This finding is in accordance with the study of Chen et al [44] which was related to distinguishing the GBM's true progression from pseudoprogression. Similar results were obtained in the study of Drabycz et al [45] where only texture features on T2W images, assessed by the space-frequency analysis, could significantly differentiate methylated from unmethylated GBM. The possible explanation might be the fact that tumor property caused by heterogeneous angiogenesis, such as ischemia, edema and necrosis, are considered more obvious on T2W images, thus, the texture features extracted from T2W potentially provided more information reflecting the vascular-related changes than did on CET1. The much longer echo time on T2W image than T1W image may underline this phenomenon [44].

The provided example (Fig. 3) shows that the most notable differences between the two tumor types were spatial frequencies of the gray tones and local homogeneity of the images. This approach (called

Table 4
Performance of Euclidean, fractal and GLCM parameters in differentiating glioblastoma from a solitary brain metastasis.

Parameters – MR images	Se (%)	Sp (%)	AUROC (±std.error)	*P*	Cut-off
Contrast (S_{CON}) - SWI	70.0	56.0	0.639 ± 0.078	0.079	242.032
Circularity ratio (M) - SWI	66.7	60.0	0.657 ± 0.073	0.046	0.835
Contrast (S_{CON}) - CET1	56.7	76.0	0.664 ± 0.074	0.038	215.180
Entropy (S_{ENT}) - T2W	76.7	64.0	0.683 ± 0.073	0.020	5.972
Normalized box dimension (D_{norm}) - CET1	66.7	72.0	0.689 ± 0.073	0.016	0.906
Entropy (S_{ENT}) - CET1	73.3	68.0	0.695 ± 0.072	0.013	6.169
Contrast (S_{CON}) - T2W	73.3	60.0	0.700 ± 0.071	0.011	358.637
Lacunarity (λ) - T2W	53.3	88.0	0.717 ± 0.070	0.006	0.278
Correlation (S_{COR}) - T2W	66.7	80.0	0.725 ± 0.071	0.004	2.841
Binary box dimension (D_{bin}) - T2W	66.7	80.0	0.726 ± 0.069	0.004	1.570
Angular second moment (S_{ASM}) – CET1	60.0	80.0	0.727 ± 0.068	0.004	0.066
Angular second moment (S_{ASM}) - SWI	63.3	76.0	0.732 ± 0.068	0.003	0.063
Normalized box dimension (D_{norm}) - T2W	63.3	84.0	0.747 ± 0.070	0.002	0.903
Perimeter (P) - SWI	66.7	80.0	0.749 ± 0.066	0.002	282.500
Angular second moment (S_{ASM}) - T2W	66.7	76.0	0.750 ± 0.066	0.002	0.0625
Surface area (A) - SWI	63.3	80.0	0.756 ± 0.066	0.001	7152.500
Space-filling ratio (SF_R) - SWI	63.3	80.0	0.756 ± 0.066	0.001	0.009
Inverse difference moment (S_{IDM}) - T2W	83.3	68.0	0.772 ± 0.063	0.001	0.433
Inverse difference moment (S_{IDM}) - CET1	66.7	84.0	0.795 ± 0.061	0.000	0.438

Se: Sensitivity; Sp: Specificity; AUROC: area under the receiver operating characteristic curve

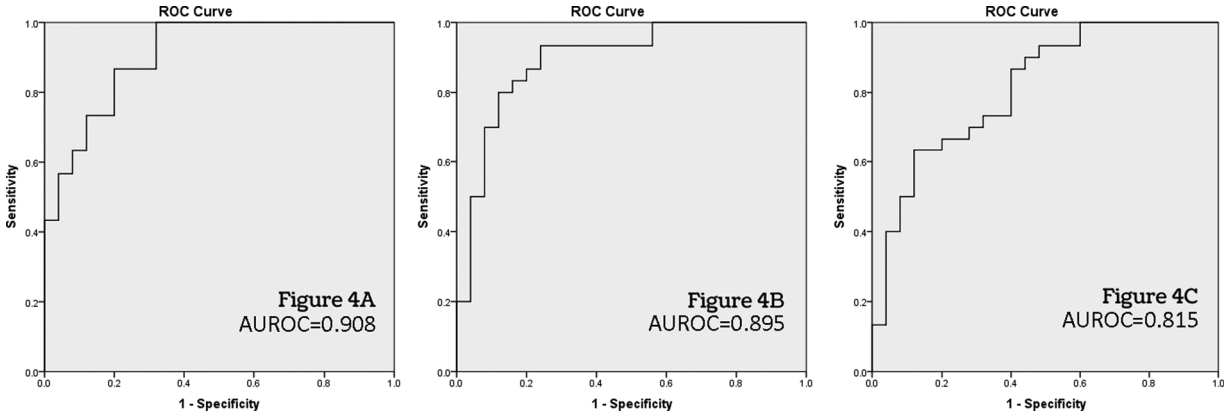

Fig. 4. ROC curves of combined selected GLCM parameters in differentiating glioblastoma from solitary brain metastasis: Fig. 4A S_{IDM}/CET1,T2W/, S_{ENT}/CET1, S_{ASM}/SWI, CET1, T2W/, S_{CON}/T2W, S_{COR}/T2W Fig. 4B S_{IDM}/T2W, S_{ASM}/T2W, S_{CON}/T2W, S_{COR}/T2W Fig. 4C S_{IDM}/CET1, S_{ENT}/CET1, S_{ASM}/CET1.

radiomics), converts the images to higher-dimensional data and can potentially aid in the improvement of decision support.

The limitations of this study were relatively small number of patients (due to the retrospective study), only one type of texture analysis and only one, but most representative slice of image analyzes per sequence (our idea was to evaluate the easiest and the fastest way of image quantifying as adding tool in daily radiological practice), absence of genetic analysis of GBM (which were only recently included in medical practice in our country for selected patients), as well as the absence of analyzes of metastases for each primary cancer separately (which was beyond the focus of interest of this paper and is certainly a good idea for further investigation). Besides mentioned, selection of regions of interest remains time-consuming and introduces an operator-dependent segmentation bias. However, the following computer-aided analysis performed on the region of interest is semiautomatic and relatively fast.

In conclusion, accurate early differentiation between GBM and solitary metastasis ensures adequate selection of further diagnostic and management procedures and leads to appropriate prognostic information. The findings of our study favor texture features as more powerful than fractal features in differentiation of these tumors, although computational multiparametric analysis might offer even more robust quantitators useful for differential diagnosis in the clinical setting.

Declaration of Competing Interest

None.

Appendix A. Supplementary data

Supplementary material related to this article can be found, in the online version, at doi:https://doi.org/10.1016/j.ejrad.2019.08.003.

References

[1] I. Tsougos, P. Svolos, E. Kousi, K. Fountas, K. Theodorou, I. Fezoulidis, et al., Differentiation of glioblastoma multiforme from metastatic brain tumor using proton magnetic resonance spectroscopy, diffusion and perfusion metrics at 3 T, Cancer Imaging 12 (2012) 423–436 https://dx.doi.org/10.1102%2F1470-7330.2012.0038.

[2] T. Abe, Y. Mizobuchi, K. Nakajima, Y. Otomi, S. Irahara, Y. Obama, et al., Diagnosis of brain tumors using dynamic contrast-enhanced perfusion imaging with a short acquisition time, Springerplus 4 (2015) 88, https://doi.org/10.1186/s40064-015-0861-6.

[3] D.O. Kamson, S. Mittal, A. Buth, O. Muzik, W.J. Kupsky, N.L. Robinette, et al., Differentiation of glioblastomas from metastatic brain tumors by tryptophan uptake and kinetic analysis: a positron emission tomographic study with magnetic resonance imaging comparison, Mol. Imaging 12 (2013) 327–337, https://doi.org/10.2310/7290.2013.00048.

[4] A. Di Ieva, F. Grizzi, H. Jelinek, A.J. Pellionisz, G.A. Losa, Fractals in neurosciences,

part I: general principles and basic neurosciences, Neuroscientist (2013) 403–417, https://doi.org/10.1177/1073858413513927.
[5] A. Di Ieva, F.J. Esteban, F. Grizzi, W. Klonowski, M. Martín-Landrove, Fractals in the neurosciences, Part II: clinical applications and future perspectives, Neuroscientist 21 (2015) 30–43, https://doi.org/10.1177/1073858413513928.
[6] A. Di Ieva, P.J. Le Reste, B. Carsin-Nicol, J.C. Ferre, M.D. Cusimano, Diagnostic value of fractal analysis for the differentiation of brain tumors using 3-Tesla magnetic resonance susceptibility-weighted imaging, Neurosurgery 79 (6) (2016) 839–846, https://doi.org/10.1227/NEU.0000000000001308.
[7] A. Di Ieva, S. Göd, G. Grabner, F. Grizzi, C. Sherif, C. Matula, et al., Three-dimensional susceptibility-weighted imaging at 7 T using fractal-based quantitative analysis to grade gliomas, Neuroradiology 55 (2013) 35–40, https://doi.org/10.1007/s00234-012-1081-1.
[8] K.M. Iftekharuddin, W. Jia, R. Marsh, Fractal analysis of tumor in brain MR images, Mach. Vision. Appl. 13 (2003) 352–362, https://doi.org/10.1007/s00138-002-0087-9.
[9] K.A. Smitha, A.K. Gupta, R.S. Jayasree, Fractal analysis: fractal dimension and lacunarity from MR images for differentiating the grades of glioma, Phys. Med. Biol. 60 (2015) 6937–6947, https://doi.org/10.1088/0031-9155/60/17/6937.
[10] A. Di Ieva, C. Matula, F. Grizzi, G. Grabner, S. Trattnig, M. Tschabitscher, Fractal analysis of the susceptibility weighted imaging patterns in malignant brain tumors during antiangiogenic treatment: technical report on four cases serially imaged by 7 T magnetic resonance during a period of four weeks, World Neurosurg. 77 (5-6) (2015), https://doi.org/10.1016/j.wneu.2011.09.006 785.e11–21.
[11] S. Liu, Y. Wang, K. Xu, Z. Wang, X. Fan, C. Zhang, et al., Relationship between necrotic patterns in glioblastoma and patient survival: fractal dimension and lacunarity analysis using magnetic resonance imaging, Sci. Rep. 8302 (2017), https://doi.org/10.1038/s41598-017-08862-6.
[12] J.H. Kim, E.S. Ko, Y. Lim, et al., Breast cancer heterogeneity: MR imaging texture analysis and survival outcomes, Radiology 282 (2017) 665–675, https://doi.org/10.1148/radiol.2016160261.
[13] S.H. Yoon, C.M. Park, S.J. Park, J.H. Yoon, S. Hahn, J.M. Goo, Tumor heterogeneity in lung cancer: assessment with dynamic contrast-enhanced MR imaging, Radiology 280 (2016) 940–948, https://doi.org/10.1148/radiol.2016151367.
[14] F. Ng, R. Kozarski, B. Ganeshan, V. Goh, Assessment of tumor heterogeneity by CT texture analysis: can the largest cross-sectional area be used as an alternative to whole tumor analysis? Eur. J. Radiol. 82 (2013) 342–348, https://doi.org/10.1016/j.ejrad.2012.10.023.
[15] D. Molina, J. Pérez-Beteta, B. Luque, E. Arregui, M. Calvo, J.M. Boras, et al., Tumour heterogeneity in glioblastoma assessed by MRI texture analysis: a potential marker of survival, Br. J. Radiol. (2016), https://doi.org/10.1259/bjr.20160242 20160242.
[16] Y. Liu, X. Xu, L. Yin, X. Zhang, L. Li, H. Lu, Relationship between glioblastoma heterogeneity and survival time: an MR imaging texture analysis, Am. J. Neuroradiol. 38 (9) (2017) 1695–1701, https://doi.org/10.3174/ajnr.A5279.
[17] M. Béresová, A. Larroza, E. Arana, J. Varga, L. Balkay, D. Moratal, 2D and 3D texture analysis to differentiate brain metastases on MR images: proceed with caution, Magn. Reson. Mater. Phys. 31 (2) (2018) 285–294, https://doi.org/10.1007/s10334-017-0653-9.
[18] B. Krstonošić, N.T. Milošević, D.L. Marić, S.S. Babović, Quantitative analysis of spiny neurons in the adult human caudate nucleus: can it confirm the current qualitative cell classification? Acta Neurol. Belg. 115 (3) (2015) 273–280, https://doi.org/10.1007/s13760-014-0365-0.
[19] E. Fernandez, H.F. Jelinek, Use of fractal theory in neuroscience: methods, advantages, and potential problems, Methods 24 (4) (2001) 309–321, https://doi.org/10.1006/meth.2001.1201.
[20] B. Mandelbrot, The fractal geometry of nature, Freeman&Co, New York, 1982.
[21] T.G. Jr Smith, G.D. Lange, W.B. Marks, Fractal methods and results in cellular morphology – dimensions, lacunarity and multifractals, J. Neurosci. Methods. 69 (2) (1996) 123–136, https://doi.org/10.1016/S0165-0270(96)00080-5.
[22] N. Milošević, The morphology of the brain neurons: box-counting method in quantitative analysis of 2D image in the fractal geometry of the brain, in: A. Di Ieva (Ed.), The Fractal Geometry of the Brain, Springer Science + Business Media, New York, 2016, pp. 109–126.
[23] N. Rajković, B. Krstonošić, N. Milošević, Box-counting method of 2D neuronal image: method modification and quantitative analysis demonstrated on images from the monkey and human brain, Comput. Math. Method. Med. (2017), https://doi.org/10.1155/2017/8967902 8967902.
[24] K. Falconer, Fractal Geometry: Mathematical Foundation and Applications, 2nd ed., John Wiley & Sons, New York, 2003.
[25] N. Rajković, D. Kolarević, K. Kanjer, N.T. Milošević, D. Nikolić-Vukosavljević, M. Radulović, Comparison of monofractal, multifractal and gray-level co-occurrence matrix algorithms in analysis of breast tumor microscopic images for prognosis of distant metastasis risk, Biomed. Microdevices 18 (2016) 83, https://doi.org/10.1007/s10544-016-0103-x.
[26] A. Karperien, H. Ahammer, H.F. Jelinek, Quantitating the subtleties of microglial morphology with fractal analysis, Front. Cell. Neurosci. 7 (3) (2013), https://doi.org/10.3389/fncel.2013.00003.
[27] R.M. Haralick, K. Shanmugam, I.H. Dinstein, Texture features for image classification, IEEE Trans. Syst. Man. Cybern. SMC-3 6 (1973) 610–621, https://doi.org/10.1109/TSMC.1973.4309314.
[28] T. Vujasinović, J. Pribić, K. Kanjer, N.T. Milošević, Z. Tomašević, Z. Milovanović, et al., Gray-level co-occurrence matrix texture analysis of breast tumor images in prognosis of distant metastasis risk, Microsc. Microanal. 21 (3) (2015) 646–654, https://doi.org/10.1017/S1431927615000379.
[29] G.J. Djuričić, M. Radulović, J.P. Sopta, M. Nikitović, N. Milošević, Fractal and gray level cooccurrence matrix computational analysis of primary osteosarcoma magnetic resonance images predicts the chemotherapy response, Front. Oncol. 7 (2017) 246, https://doi.org/10.3389/fonc.2017.00246.
[30] J.E. Cabrera, GLCM Texture Analyzer. Image J Plugin version (v0.4), Available via https://imagej.nih.gov/ij/plugins/texture.html (accessed 18 Apr 2018 (2006).
[31] T.A. Santos, C.E.B. Maistro, C.B. Silva, M.S. Oliveira, M.C. França Jr, G. Castellano, MRI Texture Analysis Reveals Bulbar Abnormalities in Friedreich Ataxia, Am. J. Neuroradiol. 36 (12) (2015) 2214–2218, https://doi.org/10.3174/ajnr.A4455.
[32] N. Mouthuy, G. Cosnard, J. Abarca-Quinones, N. Michoux, Multiparametric magnetic resonance imaging to differentiate high-grade gliomas and brain metastases, J. Neuroradiol. 39 (2012) 301–307, https://doi.org/10.1016/j.neurad.2011.11.002.
[33] L. Blanchet, P.W. Krooshof, G.J. Postma, A.J. Idema, B. Goraj, A. Heerschap, et al., Discrimination between metastasis and glioblastoma multiforme based on morphometric analysis of MR images, Am. J. Neuroradiol. 32 (1) (2011) 67–73, https://doi.org/10.3174/ajnr.A2269.
[34] R. Ortiz-Ramón, A. Larroza, S. Ruiz-España, E. Arana, D. Moratal, Classifying brain metastases by their primary site of origin using a radiomics approach based on texture analysis: a feasibility study, Eur. Radiol. 28 (2018) 4514, https://doi.org/10.1007/s00330-018-5463-6.
[35] Z. Li, Y. Mao, H. Li, G. Yu, H. Wan, B. Li, Differentiating brain metastases from different pathological types of lung cancers using texture analysis of T1 postcontrast MR, Magn. Reson. Med. 76 (5) (2016) 1410–1419, https://doi.org/10.1002/mrm.26029.
[36] J. Lee, R. Jain, K. Khalil, B. Griffith, R. Bosca, G. Rao, et al., Texture feature ratios from relative CBV maps of perfusion MRI are associated with patient survival in glioblastoma, Am. J. Neuroradiol. 37 (1) (2016) 37–43, https://doi.org/10.3174/ajnr.A4534.
[37] K. Skogen, A. Schulz, J.B. Dormagen, B. Ganeshan, E. Helseth, A. Server, Diagnostic performance of texture analysis on MRI in grading cerebral gliomas, Eur. J. Radiol. 85 (4) (2016) 824–829, https://doi.org/10.1016/j.ejrad.2016.01.013.
[38] P. Tiwari, P. Prasanna, L. Wolansky, M. Pinho, M. Cohen, A.P. Nayate, et al., Computer-extracted texture features to distinguish cerebral radionecrosis from recurrent brain tumors on multiparametric MRI: a feasibility study, Am. J. Neuroradiol. 37 (12) (2016) 2231–2236, https://doi.org/10.3174/ajnr.A4931.
[39] Z. Zhang, J. Yang, A. Ho, W. Jiang, J. Logan, X. Wang, et al., A predictive model for distinguishing radiation necrosis from tumour progression after gamma knife radiosurgery based on radiomic features from MR images, Eur. Radiol. 28 (6) (2018) 2255–2263, https://doi.org/10.1007/s00330-017-5154-8.
[40] A. Kunimatsu, N. Kunimatsu, K. Kamiya, T. Watadani, H. Mori, O. Abe, Comparison between glioblastoma and primary central nervous system lymphoma using MR image-based texture analysis, Magn. Reson. Med. Sci. 17 (1) (2018) 50–57 https://dx.doi.org/10.2463%2Fmrms.mp.2017-0044.
[41] H.B. Suh, Y.S. Choi, S. Bae, S.S. Ahn, J.H. Chang, S.G. Kang, et al., Primary central nervous system lymphoma and atypical glioblastoma: Differentiation using radiomics approach, Eur. Radiol. 28 (9) (2018) 3832–3839, https://doi.org/10.1007/s00330-018-5368-4.
[42] Z.C. Li, H. Bai, Q. Sun, Q. Li, L. Liu, Y. Zou, et al., Multiregional radiomics features from multiparametric MRI for prediction of MGMT methylation status in glioblastoma multiforme: A multicentre study, Eur. Radiol. 28 (9) (2017), https://doi.org/10.1007/s00330-017-5302-1 3640–3365.
[43] Y. Li, X. Liu, K. Xu, Z. Qian, K. Wang, X. Fan, et al., MRI features can predict *EGFR* expression in lower grade gliomas: A voxel-based radiomic analysis, Eur. Radiol. 28 (1) (2018) 356–362, https://doi.org/10.1007/s00330-017-4964-z.
[44] X. Chen, X. Wei, Z. Zhang, R. Yang, Y. Zhu, X. Jiang, Differentiation of true-progression from pseudoprogression in glioblastoma treated radiation therapy and concomitant temozolomide by GLCM texture analysis of conventional MRI, Clin. Imag. 39 (5) (2015) 775–780, https://doi.org/10.1016/j.clinimag.2015.04.003.
[45] S. Drabycz, G. Roldán, P. de Robles, D. Adler, J.B. McIntyre, A.M. Magiocco, et al., An analysis of image texture, tumor location, and MGMT promoter methylation in glioblastoma using magnetic resonance imaging, Neuroimage 49 (2) (2010) 1398–1405, https://doi.org/10.1016/j.neuroimage.2009.09.049.